*Thermophysics and Aeromechanics*, *2017*, *Vol. 24*, *No. 3*

DOI: 10.1134/S0869864317030015

# Solid particle spreading in gas-dispersed confined swirling flow. Eulerian and Lagrangian approaches*

**M.A. Pakhomov and V.I. Terekhov**

*Kutateladze Institute of Thermophysics SB RAS*, *Novosibirsk*, *Russia*

E-mails: pakhomov@ngs.ru, terekhov@itp.nsc.ru

(*Received May 17*, *2016*; *revised June 21*, *2016*)

Dynamics of a disperse phase in a swirling two-phase flow behind a sudden tube expansion is simulated with the aid of Eulerian and full Lagrangian descriptions. The carrier phase is described by three-dimensional Reynolds averaged Navier–Stokes equations with consideration of inverse influence of particles on the transport processes in gas. The velocity profiles calculated using these two approaches are practically the same. It is shown that the main difference between the Eulerian and Lagrangian approaches is presented by the concentration profile of the dispersed phase. The Eulerian approach underpredicts the value of particle concentration as compared with the Lagrangian approach (the difference reaches 15–20 %). The dispersed phase concentration predicted by the Lagrangian approach agrees with the measurement data somewhat better than the data obtained through the Eulerian approach.

**Key words:** two-phase swirling flow, solid particles, flow separation, numerical simulation, model of Reynolds stress transport, Eulerian and full Lagrangian descriptions.

## Introduction

The swirling confined two-phase flows are widely used to intensify the transport processes in various fields of technology, for example, when stabilizing the combustion process in industrial furnaces, for particle separation in cyclones, etc. The swirling flows are characterized by high local gradients of the averaged and pulsation velocities and other parameters, and they are accompanied by complex hydrodynamic phenomena arising due to the action of centrifugal Coriolis forces [1]. The recirculation flow affects the intensity of the processes of momentum, heat, and mass transfer and determines the structure of the turbulent two-phase flow [1–3]. The interaction of particles with turbulence of the carrier phase has a significant effect on dispersion of particles and their mixing with the gas flow. This is an important aspect in modeling the two-phase turbulent flows. The accounting and correct description of all these factors, which have a significant effect on the flow pattern in the swirling two-phase flow in the presence of pipe sudden expansion, are rather complicated. Therefore, despite the wide use of two-phase swirling flows in various practical applications, the processes of turbulent transport in such flows remain studied insufficiently.

Several papers on the experimental study of swirling gas-dispersed flows behind a sudden tube expansion have been published, for example, [4–6]. The studies [7–15] deal with numerical

* The work was financially supported by the grant of Russian Science Foundation (Project No. 14-19-00402).

investigation of such flows. The gas-dispersed swirling flows are considered in [10], the model of Reynolds stress transport for the two-phase flow is developed and compared with the measurement data of [4, 5]. Numerical simulation is carried out for two values of the swirl parameter $S = 0.47$ (experimental conditions of [4, 5]) and 1.5. It is shown that the agreement with the measurement results on anisotropic turbulent characteristics of the gas phase calculated by the model of Reynolds stress transport is significantly better than that calculated by the $k$–$\varepsilon$–$k_d$ model.

Two basic methods of calculation have been proposed to model dynamics of a two-phase flow [16, 17]. The first one is Eulerian continuum description (the so-called two-fluid models). The second method includes the Lagrangian trajectory approach. Both these methods have their advantages and disadvantages and complement each other. The advantages of one approach are the disadvantages of another. To describe dynamics of the dispersed phase in the two-phase turbulent flows, including those with the swirl, the Eulerian [7, 9, 15, 18] and Lagrangian [8, 10, 11, 14, 19] approaches are used.

When calculating the field of carrier phase turbulence, various modifications of two-parameter isotropic models are often used for engineering calculations [8–11, 14]. Such turbulence models, for example, the $k$–$\varepsilon$ model, have a number of serious limitations for the description of flows with swirl and rotation [20]. One of the methods that make it possible to take into account partially the complex mixing processes and anisotropy of the components of gas velocity pulsations in separated swirling flows is the use of the Second Moment Closure (SMC) models [21, 22]. For the averaged and pulsating flow characteristics, an acceptable agreement with the measurement data is obtained. There are some difficulties in describing such flows associated with the incorrect negative sign of $uw$ correlation and keeping the vortex shape of the profile of the averaged tangential velocity component at a large distance from the inlet at a small swirl parameter [20]. The model of Reynolds stress transport is successfully used to describe the turbulent characteristics of the carrier phase [15, 23–26].

To date, there are a number of papers [27, 29] devoted to comparison of possibilities of the Eulerian and Lagrangian descriptions of the two-phase flows with solid particles or drops for different types of the flows. Calculations [27, 28] of separated gas-dispersed flow behind a sudden expansion of the flat channel [27] and sudden expansion of the tube [28] by the Reynolds-averaged Navier–Stokes (RANS) equations did not show the distinct advantages of one approach over another both in the averaged and pulsation parameters of the two-phase flow. Numerical study of dispersed phase flow, turbulence, and heat transfer in the turbulent gas-droplet flow behind a sudden expansion of the tube was performed in [29] using the Eulerian and Lagrangian methods. It was shown that the main difference between these approaches is shown by the droplet concentration profiles.

Thus, the question of the advantage of one approach over another in the study of swirling two-phase flows in the presence of a sudden expansion remains open until now. In this work, an attempt to obtain a partial answer to this question was made by comparing the calculated data with results of known measurements [4, 5] included into the ERCOFTAC database.

## Computational methods for the two-phase flows

In this paper, we compare the capabilities of the Eulerian and Lagrangian methods for calculating dynamics of a dispersed phase to describe a swirling two-phase turbulent flow behind a sudden expansion of the tube. In the Lagrangian (trajectory) approach, the deterministic motion of a representative set of particles along the individual trajectories (not less than several thousand) is described in the Lagrangian variables, and the motion of carrier medium is described in the Eulerian variables. Equations describing the motion of the discrete phase are integrated along the individual trajectories in the field of the carrier medium calculated in advance. Then, the solutions are averaged over the entire data ensemble. As the particle size decreases, the number of implementations should increase because contribution of their

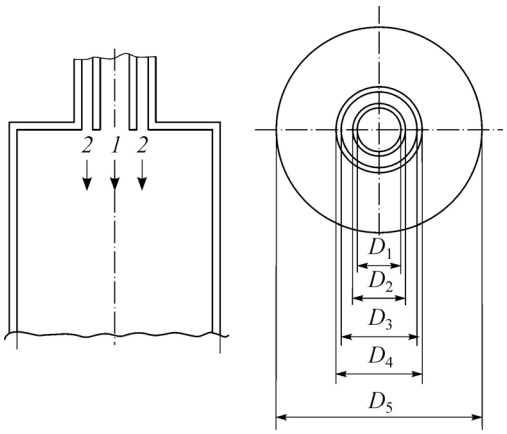


*Fig. 1*. Scheme of experimental setup [4, 5].
*1* — non-swirling gas-dispersed flow,
*2* — swirling gas flow.

interactions with the smaller vortices of the gas phase increases. In the Eulerian (two-fluid) method, the equations of one type and single numerical algorithm are used for both phases. Description of very small particles does not cause any fundamental difficulties because at $d \to 0$, the passage to the limit of inertia-free impurity flow occurs, where $d$ is the size of the dispersed phase.

In the present study, the problem of dynamics of the two-phase swirling turbulent gas-dispersed flow is considered. The solution uses a system of stationary RANS equations written with consideration of the inverse influence of particles on the transport processes in the gas phase in the averaged and pulsating motions. A schematic representation of the flow is shown in Fig. 1. Calculations are carried out for the vertical turbulent two-phase flow of the descending direction. A non-swirling jet of the air and glass particles mixture *1* is fed into the central cylindrical channel ($2R_1 = D_1$), and the swirling single-phase airflow *2* passes through the peripheral annular channel $(R_3 - R_2) = (D_3 - D_2)/2$. The volume concentration of dispersed phase is very small, it is $\Phi = M_\mathrm{d}\rho/\rho_\mathrm{d} = 1.6\cdot10^{-5}$, the particles are sufficiently small ($d_1 < 100$ μm), so we can neglect the effects of their collisions with each other. Here, $M_\mathrm{d}$ is the mass concentration of particles, and $\rho$ and $\rho_\mathrm{d}$ are the densities of gas and particle material.

It should be noted that all equations below are written in the tensor form applied in the Cartesian coordinate system only for the sake of their compactness. Equations have a form suitable for describing the axisymmetric flow.

**System of averaged equations of the gas phase**

The stationary three-dimensional RANS equations taking into account the back influence of particles on the processes of mean and fluctuational transport in gas are used in this study:

$$\rho\frac{\partial U_j}{\partial x_j} = 0,$$

$$\frac{\partial\left(U_iU_j\right)}{\partial x_j} = -\frac{\partial\left(P+2k/3\right)}{\rho\partial x_i} + \frac{\partial}{\partial x_j}\left(\nu\frac{\partial U_i}{\partial x_j} - \left\langle u_iu_j\right\rangle\right) - \left(U_i - U_{\mathrm{d},i}\right)\Phi\frac{\rho_\mathrm{d}}{\tau\rho} + S_i, \qquad (1)$$

here $U_i$ ($U$, $V$, and $W$) and $u_i$ ($u$, $v$, and $w$) are axial, radial, and tangential components of averaged and pulsation velocities, respectively, $\nu$ is the coefficient of kinematic viscosity, $x_i$ are projections on the coordinate axes, $2k = \left\langle u_iu_i\right\rangle = \left\langle u^2\right\rangle + \left\langle v^2\right\rangle + \left\langle w^2\right\rangle$ is kinetic energy of gas phase turbulence, $P$ is the pressure, $\tau = \rho_\mathrm{d}d^2/(18\rho\nu W)$ is the time of dynamic relaxation of particles with consideration of deviation from the Stokes flow law, $W = 1 + \mathrm{Re}_\mathrm{d}^{2/3}/6$, $\mathrm{Re}_\mathrm{d} = \left|\mathbf{U} - \mathbf{U}_\mathrm{d}\right|d/\nu$ is the Reynolds number of dispersed phase derived by the interfacial velocity, $d$ is the particle diameter, $S_i$ is the effect of flow swirl ($S_U = 0$, $S_V = W^2/r - \nu V/r^2 + \left\langle w^2\right\rangle/r$, $S_W = -VW/r - \nu W/r^2 + \left\langle vw\right\rangle/r$ [20]), index d corresponds

to the dispersed phase. All equations of system (1) are written with consideration of dispersed phase effect on the processes of momentum transfer in the gas flow.

**Model of Reynolds stress transport**

Gas phase turbulence $\langle u_i u_j \rangle$ and rate of its dissipation $\varepsilon$ were simulated using the model of Reynolds stress transport [30, 31]:

$$\frac{\partial\left(U_k \left\langle u_i u_j \right\rangle\right)}{\partial x_k} = P_{ij} + \phi_{ij} - \varepsilon_{ij} + \frac{\partial}{\partial x_k}\left(\nu\delta_{kl} + \frac{C_\mu T_\mathrm{T}}{\sigma_k}\left\langle u_k u_l \right\rangle\right)\frac{\partial}{\partial x_l}\left\langle u_i u_j \right\rangle - A_{\mathrm{d},i},$$

$$\frac{\partial\left(U_k \varepsilon\right)}{\partial x_k} = \frac{1}{T_\mathrm{T}}\left(C_{\varepsilon 1}\tilde{P} - C_{\varepsilon 2}\varepsilon\right) + \frac{\partial}{\partial x_k}\left(\nu\delta_{kl} + \frac{C_\mu T_\mathrm{T}}{\sigma_\varepsilon}\left\langle u_k u_l \right\rangle\right)\frac{\partial \varepsilon}{\partial x_l} - \varepsilon_{\mathrm{d},i},$$

$$\beta - L_\mathrm{T}^2 \nabla^2 \beta = 1, \tag{2}$$

here $P_{ij} = -\left\langle u_i u_j \right\rangle \frac{\partial U_j}{\partial x_i} - \left\langle u_i u_j \right\rangle \frac{\partial U_i}{\partial x_j}$ is the intensity of energy transfer from the averaged motion to pulsation; $\tilde{P} = 0.5 P_{ii}$, $T_\mathrm{T} = \max\left(k/\varepsilon;\ C_T\sqrt{\nu/\varepsilon}\right)$ and $L_\mathrm{T} = C_L \max\left(k^{3/2}/\varepsilon;\ C_\eta \sqrt[4]{\nu^3/\varepsilon}\right)$ are time and geometric macroscales of turbulence, respectively [30]; $\phi_{ij} = \left(1-\beta^2\right)\phi_{ij}^\mathrm{W} + \beta^2 \phi_{ij}^\mathrm{H}$ is the redistributing term, which describes energy exchange between separate components $\left\langle u_i u_j \right\rangle$ due to pressure–deformation rate correlation [30], $\varepsilon$ is the dissipation or rate of energy transfer from the large-scale vortices to the small-scale ones, and $\beta$ is the mixing ratio determined from the elliptical equation and used for calculation of the redistributing term [30], it varies from zero on the wall to one at some distance from the wall, $\phi_{ij}^\mathrm{W}$ is "inhomogeneous" part of the redistributing term (in the near-wall region), and $\phi_{ij}^\mathrm{H}$ is "homogeneous" part of the redistributing term (far from the wall) [31], index T corresponds to the turbulent term. The redistributing term is written taking into account the effect of two-phase character of the flow [25].

Last terms $A_\mathrm{d}$ and $\varepsilon_\mathrm{d}$ in the right-hand sides of equations of system (2) take into account the inverse influence of particles on the carrier phase due to pulsation interfacial sliding [32, 33], $A_{\mathrm{d},i} = \frac{2\rho_\mathrm{d}\Phi}{\rho\tau}\left(1-f_u\right)\left\langle u_i u_i \right\rangle$, $\varepsilon_{\mathrm{d},i} = \frac{2\rho_\mathrm{d}\varepsilon}{\rho\tau}\left[\Phi\left(1-f_\varepsilon\right)\right]$, where $f_u$ and $f_\varepsilon$ are the coefficients of particle involvement into turbulent motion of gas [32].

The constants and functions of the SMC-model of turbulence in system (2) are presented in [30]: $C_\mu = 0.22$, $C_{\varepsilon 1} = 1.44\left[1 + 0.03\left(1-\beta^2\right)\sqrt{\frac{k}{\left\langle u_i u_i \right\rangle n_i n_j}}\right]$, $C_{\varepsilon 2} = 1.85$, $\sigma_k = 1$, $\sigma_\varepsilon = 1.22$, $C_T = 0.161$, $C_L = 6$ and $C_\eta = 80$.

**Eulerian approach**

The system of averaged equations describing the transport processes in the dispersed phase takes the form [15]

$$\frac{\partial\left(\Phi\rho_{\mathrm{d}}U_{\mathrm{d},j}\right)}{\partial x_j}=0,$$

$$\frac{\partial\left(\rho_d\,\Phi U_{d,j}\,U_{d,i}\right)}{\partial x_j}+\frac{\partial\left(\rho_{\mathrm{d}}\Phi\left\langle u_{\mathrm{d},i}u_{\mathrm{d},j}\right\rangle\right)}{\partial x_j}=\Phi\left(U_i-U_{\mathrm{d},i}\right)\frac{\rho_{\mathrm{d}}}{\tau}+\Phi\rho_{\mathrm{d}}g-\frac{1}{\tau}\cdot\frac{\partial\left(\rho_{\mathrm{d}}D_{\mathrm{d},ij}\Phi\right)}{\partial x_j},\qquad(3)$$

where $D_{\mathrm{d},ij}$ is the tensor of turbulent diffusion of particles [32, 33], and equations of the second moments of velocity pulsations $\left\langle u_{\mathrm{d},i}u_{\mathrm{d},j}\right\rangle$ take the same form as in [32, 33]. The system of equations (3) with corresponding boundary conditions allows us to predict the motion and concentration of the dispersed phase in the swirling turbulent flow.

**Full Lagrangian description**

The equation of gas phase motion has the same form as in the Eulerian approach. In the Lagrangian method, the effect of particles on the carrier gas flow is determined using the approach described in [34]. In this case, the transition from the results of calculating the trajectories to distributions of disperse phase parameters in physical space (for example, when calculating droplet concentration) is carried out by averaging these results by the control volume of the Eulerian grid used for gas phase calculation.

When calculating particle dynamics, the SSF model (Stochastic Separated Flow) [35], taking into account the stochastic effect of gas turbulence on particle motion, is usually used. Instantaneous (actual) gas velocity $\tilde{U}_i=U_i+u_i'$ determined as the sum of averaged $U_i$ (determined directly from RANS calculation) and random pulsating $u_i'$ velocity components is used as the characteristic velocity of gas in the model. Random pulsation value $u_i'=\xi\sqrt{k}$ is determined using Gaussian function $\xi$, whose mean value is zero, and standard deviation is one. The smallest value of the vortex lifetime and time of particle interaction with the turbulent vortex is chosen as the criterion for generating the random component of the gas velocity. This means that the gas phase affects turbulent dispersion of particles only at the points corresponding to the instant of interaction beginning along the entire trajectory of the dispersed phase motion. Interaction is considered as a discrete process, therefore, to obtain the statistically reliable solution along the dispersed phase trajectory, it is necessary to carry out a large number of computations of particle trajectories (the order of $10^4$). The simple and reliable SSF model was used for calculations of the two-phase flows of various types, for example, in [8, 10, 11, 27, 28]. Its main drawback relates to the fact that the pulsating field of the gas velocity is not continuous; in addition, the fact that turbulent pulsations are correlated in time and space is not taken into account [36].

There are several modified SSF models, for example, ISSF (Improved Stochastic Separated Flow) [36], whose main difference from the SSF-model is the use of much smaller number of calculated particles (about $10^2$–$10^3$) and the fact that interfacial interaction is a continuous process. The averaged phase velocity is used in the equations of motion. The random rms pulsations of the disperse phase are predicted along the stochastic trajectory, and this allows us to maintain the stochastic character of dispersed phase motion. This approach was used by the authors of the present work in [29] when comparing the Eulerian and Lagrangian methods for describing the two-phase separated flows without swirling.

**Calculation of dispersed phase position and velocity by the Lagrangian method**

Coordinates $\mathbf{x}_{\mathrm{d}}$ and the dispersed phase velocity components $\mathbf{U}_{\mathrm{d}}$ are computed by equations:

$$\frac{d\mathbf{x}_\mathrm{d}}{dt} = \tilde{\mathbf{U}}_\mathrm{d}, \tag{4}$$

$$m_\mathrm{d}\frac{d\tilde{\mathbf{U}}_\mathrm{d}}{dt} = \mathbf{F}_\mathrm{D} + \mathbf{F}_\mathrm{P} + \mathbf{F}_\mathrm{S} + \mathbf{F}_\mathrm{g}, \tag{5}$$

where $x_{\mathrm{d},i}$ are the components of particle coordinate determined along the stochastic trajectory, $\tilde{\mathbf{U}}_\mathrm{d}$ is the instantaneous velocity of dispersed phase, $m_\mathrm{d} = \rho_\mathrm{d}\pi d^3/6$ is the mass of particle; $d$ and $\rho_\mathrm{d}$ are particle diameter and material density, respectively, $\mathbf{F}_\mathrm{D}$ is the drag force, $\mathbf{F}_\mathrm{P}$ is the force taking into account the pressure gradient of the carrier medium, $\mathbf{F}_\mathrm{S}$ is the Saffman force, and $\mathbf{F}_\mathrm{g}$ is gravity. The influence of particle rotation, virtual mass force, and Basset force on dynamics of particle motion in equation (5) can be neglected. The drag is determined by formula $\mathbf{F}_\mathrm{D} = 1/8\cdot\rho\pi d^2 C_\mathrm{D}(\mathbf{U}_\mathrm{S} - \tilde{\mathbf{U}}_\mathrm{d})\left|\mathbf{U}_\mathrm{S} - \tilde{\mathbf{U}}_\mathrm{d}\right|$, here $C_\mathrm{D} = \frac{24}{\mathrm{Re}_\mathrm{d}}\left(1 + 0.15\,\mathrm{Re}_\mathrm{d}^{2/3}\right)$ is the coefficient of solid sphere drag at $\mathrm{Re}_\mathrm{d} < 1000$ written with consideration of deviation from the Stokes flow law; $\mathrm{Re}_\mathrm{d} = d\left|\mathbf{U}_\mathrm{S} - \tilde{\mathbf{U}}_\mathrm{d}\right|/\nu$ is the Reynolds number of dispersed phase, $\rho$ is the density of the gas phase; $\mathbf{U}_\mathrm{S} = \mathbf{U}\left(\mathbf{x}_\mathrm{P}(t), t\right)$ is the gas velocity at the point of solid particle location (so-called gas velocity seen by particles).

Pressure gradient of carrier medium $\mathbf{F}_\mathrm{P}$, the radial force (Saffman force) $\mathbf{F}_\mathrm{S}$ [37], and the gravity force $\mathbf{F}_\mathrm{g}$ are calculated by relationships:

$$\mathbf{F}_\mathrm{P} = -m_\mathrm{d}\frac{\rho}{\rho_\mathrm{d}}\cdot\frac{D\mathbf{U}}{Dt}, \quad \mathbf{F}_\mathrm{S} = 1.615 d^2\rho\left(\mathbf{U}_\mathrm{S} - \tilde{\mathbf{U}}_\mathrm{d}\right)\sqrt{\nu\left|\frac{d\mathbf{U}}{dx}\right|}, \quad \mathbf{F}_\mathrm{g} = m_\mathrm{d}\mathbf{g}.$$

The pulsation velocity of particle is determined from the algebraic relationship presented in [38]:

$$\left\langle u_{\mathrm{d},i}u_{\mathrm{d},j}\right\rangle = f_u\left\langle u_i u_j\right\rangle = \frac{\Omega_\mathrm{LP}}{\tau + \Omega_\mathrm{LP}}\left\langle u_i u_j\right\rangle, \tag{6}$$

where $\Omega_\mathrm{LP}$ is the time of particle interaction with energy-intensive fluctuations of the gas phase [32, 33]. For the case of low-inertial particles, it can be assumed that $\Omega_\mathrm{LP} \approx \Omega_\mathrm{L}$ [32, 33], then $\left\langle u_{\mathrm{d},i}u_{\mathrm{d},j}\right\rangle \approx \frac{\Omega_\mathrm{L}}{\tau + \Omega_\mathrm{L}}\left\langle u_i u_j\right\rangle$, where $\Omega_\mathrm{L} = 0.482k/\varepsilon$ is the turbulent time scale [39].

**Calculation of gas phase velocity at the point of particle location**

To model the gas phase velocity at the point of particle location, the following approach is used [40]

$$\mathbf{U}_{\mathrm{S},i} = \mathbf{U}_i + \mathbf{u}_{\mathrm{S},i}, \tag{7}$$

where $\mathbf{U}_i$ and $\mathbf{u}_{\mathrm{S},i}$ are the averaged (determined by the RANS calculation) and pulsating velocity of gas at particle location, respectively. In English-language publications, this parameter is called "dispersion modeling" [39–42]. One of the ways to predict it is the Continuous Random Walk model (see [41]):

$$u_{\mathrm{S},i}^m = a_{ij}u_{\mathrm{d},j}^{m-1} + b_{ij}\zeta_j + A_i\Delta t, \quad \zeta_i \in N(0,\,1). \tag{8}$$

Here the superscript $m$ refers to the current time step, $N(0, 1)$ is a random Gaussian value distributed with an average value of zero and standard deviation of one, $\mathbf{A}$ is the vector of the corrected bias, and $\Delta t$ is the time step. The tensors of displacement $\mathbf{a}$ and diffusion $\mathbf{b}$ are determined from the following relationships given in [40]:

$$a_{ij} = \exp\left(-\frac{\Delta t}{\tau_{S,i}}\right)\delta_{ij}, \quad b_{ik}b_{jk} = \left(1 - a_{ii}a_{jj}\right)u_{ij}.$$

When calculating the turbulent scales, dispersed modeling uses relationships of [42]: $\tau_{\mathrm{S},\parallel} = \dfrac{\left(\beta^*/\beta\right)\Omega_L}{1+m\beta^*\zeta}$, $\tau_{\mathrm{S},\perp} = \dfrac{\left(\beta^*/\beta\right)\Omega_L}{1+2m\beta^*\zeta}$, where $\beta^* = \left[\left(1+\tau/\Omega_L\right)^{-0.5}\left(\beta^{-1}-1\right)+1\right]^{-1}$ and $\zeta = \dfrac{\mathbf{U}-\mathbf{U}_\mathrm{d}}{\sqrt{u_i u_j}}$, here $m = 1$ is the structural parameter, $\beta = 0.356$ [40], $i = \parallel$ and $i = \perp$ are directions parallel and normal to $\mathbf{U}-\mathbf{U}_\mathrm{d}$, respectively.

To calculate the components of corrected bias vector **A**, relationships from [43] are used: $A_{ij} = \dfrac{1}{1+\mathrm{St}_\mathrm{d}}\left[\dfrac{1}{\rho}\cdot\dfrac{\partial}{\partial x_j}\left(\rho\left\langle u_i u_j\right\rangle\right)\right]$, where $\mathrm{St}_\mathrm{d} = \dfrac{\tau}{1/7\left(k/\varepsilon\right)}$ is the Stokes number in the large-scale turbulent motion.

**Calculation of particle concentration**

An important aspect of the Euler-Lagrangian approach is the calculation of dispersed phase concentration. To do this, we use the procedures of spatial [34] or spatial-temporal [35] averaging of results by all particle trajectories over the control volume of the Euler grid used for calculation of the gas phase field.

Another approach to calculating the dispersed phase parameters is the use of so-called full Lagrangian method [44]. This method is based on the use of additional equations for the components of Jacobian transition from Eulerian to Lagrangian variables. Disperse phase concentration is computed from the continuity equation written in the Lagrangian form. The main advantage of this approach is that all parameters of the dispersed phase, including concentration, are found from solutions to the systems of ordinary differential equations on the selected particle trajectories. This approach eliminates the need to average the particle trajectories over a small physical control volume, leads to a significant decrease in the required number of particle trajectories, and removes almost insoluble problem of invariance of the obtained solution with respect to the shape and size of the applied grid. It will be used by the authors in this paper.

The system of equations for determining the parameters of particles on a fixed trajectory consists of the equation of continuity for the mass of particles written with consideration of vaporization on the surface of evaporating droplets, equations of particle motion written in Lagrangian variables, and additional equations for finding the Jacobian components in the continuity equation [44]. The algebraic equation of the balance of numerical concentration of the dispersed phase $n$ in Lagrangian variables has the form:

$$n = n_0 / \left|J_\mathrm{EL}\right|, \tag{9}$$

where $n$ is the numerical concentration of particles at the current moment, $n_0$ is the numerical concentration of particles at $t = 0$ and $\left|J_\mathrm{EL}\right|$ is the Jacobian module at transition from the Eulerian to Lagrangian coordinates [44].

Equations (4–9) are numerically integrated along the trajectories of particle motion. The components of the averaged velocity of the dispersed phase in the system of equations (5) are predicted taking into account (7). Numerical concentration of particles is calculated from equation (9). The boundary conditions for the Jacobian in the case of two-dimensional stationary two-phase flow are considered in [45].

### Methods of numerical implementation

The technique of numerical implementation is described in detail in [15, 29]. The components of Reynolds stresses of the gas phase were determined according to the approach proposed in [46]. All calculations were carried out using a grid of $200\times80\times80 = 1.28\cdot10^6$ control volumes. A further increase in their number did not significantly affect the results of numerical calculations. The length of computational domain was $X = 1$ m.

The conditions of conjugation smoothness for both phases were set on the tube axis in the Eulerian formulation. For the dispersed phase, the boundary conditions described in [33] were used on the channel wall. As in [15, 29], it was assumed that the particles are reflected from the wall with the reduction coefficient of 0.8. The conditions of zero derivatives of all sought parameters in axial direction were set in the outlet cross section. The inlet parameter distributions were set using experimental data [4, 5]. In the absence of the required measurement results, they were determined based on the assumption of uniform distribution of the unknown parameters over the tube cross section. To determine the initial values of radial averaged phase velocities, we used the relationships for the law of solid body rotation given in [9]: $V_1 = 4SU_{m1}r/R$, $V_{d1} = 4S_dU_{d1}r/R$, where $S = \int_0^{R_3} \rho U_1 W_1 r^2 dr \Big/ \int_0^{R_3} \rho U_1^2 r dr$ is the parameter of airflow swirl, and $S_d = \int_0^{R_3} \rho_d U_{d1} W_{d1} r^2 dr \Big/ \int_0^{R_3} \rho_d U_{d1}^2 r dr$ is parameter of dispersed phase flow swirl.

At the first stage, comparisons with the measurement data of [47] were made for a single-phase air swirling flow in a tube with sudden expansion. Good agreement between the predicted and measured data was obtained for the average and pulsation characteristics (the difference did not exceed 15%), and this served as the basis for calculating the two-phase gas-dispersed flow using the Reynolds stress transport model.

### Analysis of results and discussion

Numerical calculations were carried out for the measurement conditions [4, 5]. Geometry of experimental section was as follows: $2R_1 = D_1 = 32$ mm, $2R_2 = D_2 = 38$ mm, $2R_3 = D_3 = 64$ mm, $2R_4 = D_4 = 70$ mm, and $2R_5 = D_5 = 194$ mm, the step height was $H = 65$ mm (see Fig. 1). The main non-swirling jet of the mixture of gas and glass particles was fed through the axial hole, the swirling air jet was fed through the annular opening. The mass flow rate of the main gas jet $G_1$ was 9.9 g/s, the flow rate of the secondary annular jet $G_2$ was 38.3 g/s. The parameter of flow swirl changed in the range of $S = 0$–$1$. Reynolds number was $\mathrm{Re} = U_m 2R_3/\nu = 5.24\cdot10^4$, the average initial air flow velocity was $U_{m1} = 12.9$ m/s, the diameter of glass particles varied in the range of $d = 30$–$100$ μm, their mass concentration was $M_d = 0.034$. The temperature of air and particles was 300 K, gas density was $\rho = 1.18$, particle density was $\rho_d = 2500$ kg/m$^3$. The criterion characterizing the degree of particle entrainment into the gas phase motion is the Stokes number of the averaged motion: $\mathrm{Stk} = \tau/\tau_f$, where $\tau_f$ is the turbulent time macroscale. According to the data of [48], $\tau_f = 5H/U_{m1} = 0.025$ s, taking into account that $\tau = 6.9\cdot10^{-3} - 0.01$ s, we obtain $\mathrm{Stk} \approx 0.3$–$3$. This suggests that the particles can be involved into the turbulent motion of gas at $\mathrm{Stk} < 1$, and do not interact with it at $\mathrm{Stk} > 1$ [49].

The profiles of the averaged velocity components of the gas phase at calculating the velocities of dispersed phase components in terms of the Eulerian and Lagrangian approaches practically do not differ from each other, and this agrees with the authors' earlier calculations on the swirling two-phase flow behind a sudden tube expansion [29]. Therefore, they are not presented in the current work.

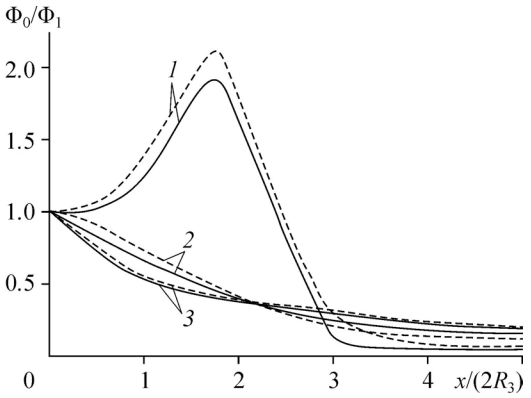


*Fig. 2*. Change in volumetric concentration of dispersed phase along the tube axis. Solid lines — Eulerian approach, dashed lines — full Lagrangian approach; $M_d = 0.034$, $S = 0.47$; $d = 30$ (*1*), 45 (*2*), 100 (*3*) μm.

Data of numerical calculations on distribution of dispersed phase volume concentration along the tube axis are shown in Fig. 2 and in several cross sections from the cross section of flow separation (Fig. 3), depending on a change in particle diameter. Here $\Phi_0$, $\Phi$, and $\Phi_1$ are the volume concentrations of particles on the tube axis in the considered control volume and in the inlet cross section, respectively. The difference in the size of dispersed particles leads to significant differences in distribution of particle concentration in the separation zones of the swirling gas-dispersed flow. For small particles ($d$ = 30 μm), a sharp increase in dispersed phase concentration in the initial cross sections is observed due to its accumulation in the region of recirculation under the action of reverse flows. Non-uniformity of the profile of turbulent kinetic energy of the gas and dispersed phases along the tube radius leads to turbulent migration of particles (turbophoresis force) towards the tube axis [49, 50]. This causes the maximum of solid particle concentration on the channel axis in the case of small particles ($d$ = 30 μm). For the most inertial particles ($d$ = 100 μm), rapid scattering of dispersed phase over the channel cross section due to the action of centrifugal forces and turbulent diffusion and migration is characteristic. These conclusions are consistent with the measurement data [4, 5] and numerical calculations for the swirled two-phase flows in the presence of separation zones given in [12, 49].

The effect of gas flow swirl on a change in dispersed phase concentration along the tube axis and over its cross section in the two-phase gas-dispersed flow is shown in Fig. 4. An increase in the number of particles on the tube axis due to centrifugal forces is characteristic of the swirling flow (see Fig. 4*a*), whereas in the near-wall region, the value of dispersed phase concentration is negligibly small. This effect becomes more pronounced with increasing

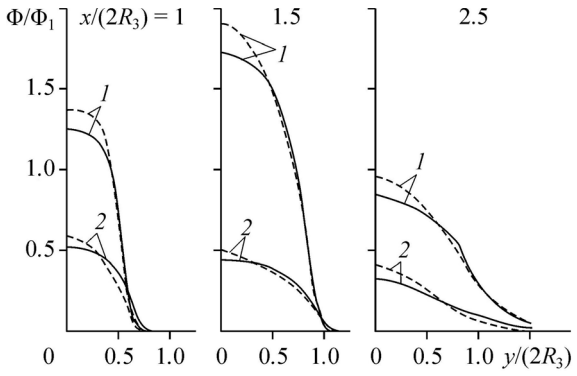


*Fig. 3*. Profiles of volumetric concentration of particles along the tube with varying size of dispersed phase particles in the swirling flow. $M_d = 0.034$, $S = 0.47$; $d = 30$ μm (*1*), 100 μm (*2*).

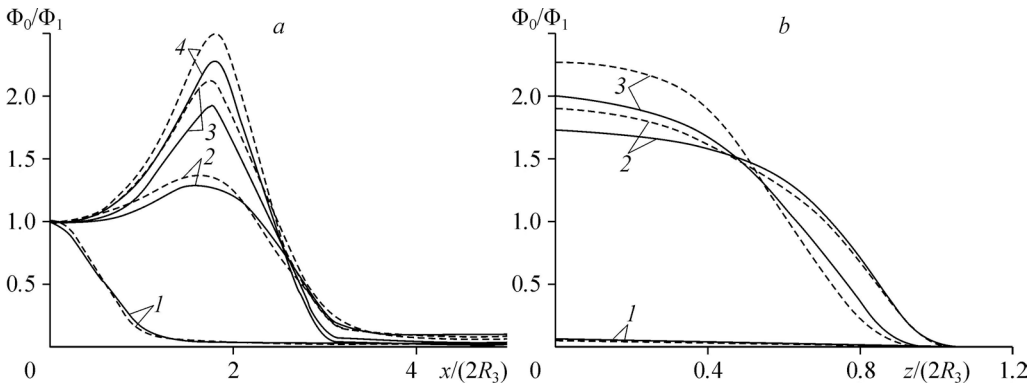


*Fig. 4*. Effect of the parameter of flow swirl on distribution of volumetric concentration of dispersed phase along the tube axis (*a*) and over its cross section (*b*) at $x/(2R_3) = 1.5$.

Solid lines — Eulerian approach, dashed lines — full Lagrangian approach; $M_d = 0.034$, $d = 30$ μm; $S = 0$ (*1*), 0.2 (*2*), 0.47 (*3*), 1 (*4*).

value of the swirl parameter. Distribution of particles over the tube cross section also has a non-monotonic character (see Fig. 4*b*). For the two-phase flow without swirl at S = 0 (line 1), rapid scattering of particles over the tube cross section after the cross section of a sudden expansion is characteristic, and this leads to a sharp decrease in dispersed phase concentration in the axial zone of the tube [49].

We should note several general conclusions by the analysis of results shown in Figs. 2–4. In general, calculation by the Eulerian and Lagrangian methods for swirling two-phase confined flows yields qualitatively similar results. The maximal difference does not exceed 15–20 %. The Lagrangian calculation gives an overestimated value of particle concentration in the axial region of the tube in comparison with the Eulerian approach under the action of turbophoresis force and accumulation of particles in the zone of reverse flows. Accordingly, when moving towards the wall, the value of concentration determined by the Lagrangian method is underestimated, when compared with the value simulated by the Eulerian approximation. Therefore, the results of numerical calculations were further compared with the measurement data [4, 5], where the radial profiles of the mass flux of dispersed phase were shown in several cross sections behind a sudden tube expansion.

### Comparison with measurement results

For comparison, the known experimental data were used [4, 5]. The swirling two-phase flow was investigated in the descending regime after a sudden expansion of the tube (see the diagram of experimental setup in Fig. 1). The measurements were performed using a single-component phase Doppler anemometer at distances $x$ = 52, 112, 195 and 315 mm ($x/(2R_3)$ = 0.81, 1.75, 3.05, and 4.92) from the cross section of sudden tube expansion. Note that calculation began with distance $x$ = 3 mm from the separation cross section. In this section, the data of measurements are given, which were used as the input ones for numerical simulation. The average diameter of glass particles $d$ in experiments [4, 5] determined by their number in the unit volume (mean number) was 45 μm, the particle size varied from 0 to 123.8 μm.

Data of comparative analysis of numerical calculations and measurements for the averaged radial $V$ and $V_d$ components of the phase velocities are shown in Fig. 5. For cross section $x$ = 315 mm, there are no experimental data for the particles in the axial zone of the tube because of their low velocity in this flow region [4, 5]. In the initial cross section located at the distance of 3 mm from the cross section of the sudden tube expansion, the averaged phase

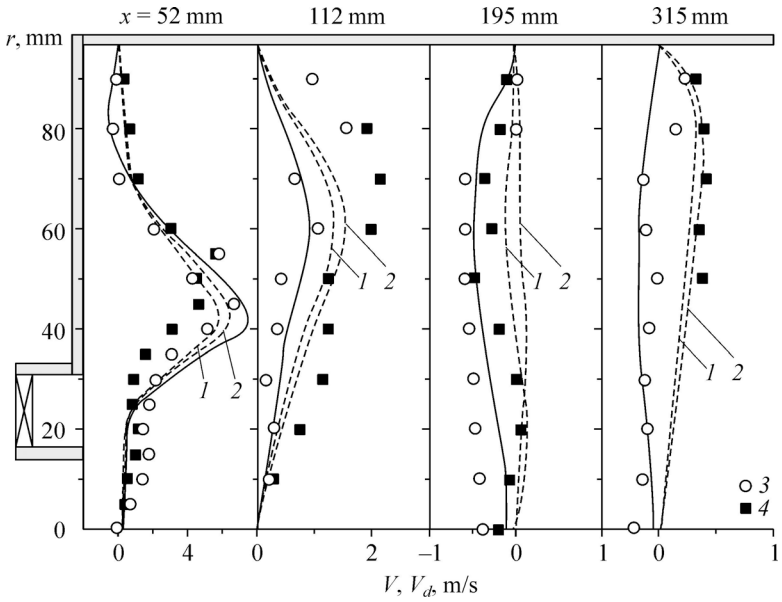


*Fig. 5.* Profiles of averaged radial phase velocities.

Points — measurements of [4, 5], lines — data of the current calculation:
solid lines — gas phase, dashed lines — particles;
*1* — Eulerian approach, *2* — full Lagrangian approach, *3* — gas, *4* — particles; $M_d = 0.034$ and $S = 0.47$.

velocities have the same values. The axial averaged velocity of gas was calculated by the data of modeling the dispersed phase velocity only by the Eulerian method. Results of both approach application give a somewhat lower value of phase velocities for particles than the measurement data [4, 5]. The radial velocity profiles of gas and dispersed phases have the expected maximum in the mixing layer in the first two cross sections at $x$ = 52 and 112 mm. We should note that there is a satisfactory agreement between the results of measurements and numerical simulation over the entire length of the calculation area. A good agreement with calculations of [8, 12] is also found for the averaged particle velocity fields. These data are not shown in Fig. 4, to provide obvious presentation of results. Comparison of the Eulerian and Lagrangian methods shows that the results of their application agree well with the measurement data [4, 5] (the difference does not exceed 10–15%). It can be noted that the Lagrangian method overestimates slightly the particle velocity in comparison with the Eulerian approach.

The radial profiles of the measured [4, 5] and predicted mass flux of particles along the axial coordinate are shown in Fig. 6. The mass flux was calculated by the following relationship: $F = \rho_d U_d M_d$, where $\rho_d$, $U_d$, and $M_d$ are the density of particle material, its averaged axial velocity, and mass concentration, respectively. As we move from the inlet cross section, a significant rearrangement of the profile of dispersed phase mass flux over the tube cross section is observed. There is a noticeable maximum of dispersed phase flow in the axial zone of the tube, and it is kept up to distance $x$ = 195 mm from its sudden expansion. Starting from the second cross section ($x$ = 112 mm), the dispersed phase accumulates in the near-wall part of the cylindrical channel as a result of an increase in the tangential velocity of particles and turbophoresis force action, which agrees with the results of [4, 5]. Excluding the near-axis zone, a good agreement between the obtained data and measurement results can be noted [4, 5].

In cross section $x$ = 315 mm, experimental data are given only for the near-wall region, since in the axial region, the particles move to the tube periphery due to centrifugal forces, and their number is insufficient to obtain reliable results by the method of phase Doppler anemometry. In the first three cross sections ($x$ = 52, 112 and 195 mm), a decrease in dispersed

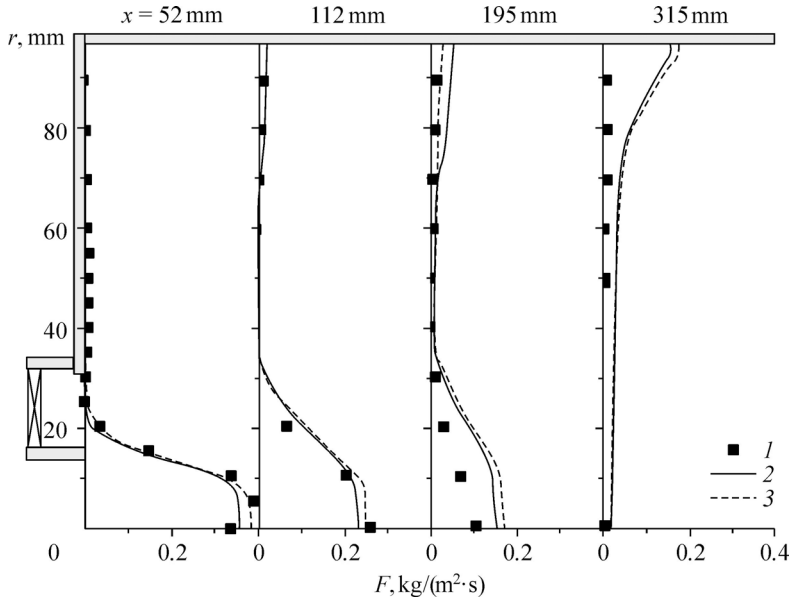


*Fig. 6*. Radial distributions of the mass flux of particles in separated swirling two-phase flow. Measurement data of [4, 5] (*1*), calculation of the authors: Eulerian (*2*) and full Lagrangian (*3*) approaches; $d = 45$ μm, $M_d = 0.034$, and $S = 0.47$.

phase concentration occurs faster than it is observed in experiments. Accordingly, this leads to an increase in the number of particles in the near-wall region of the channel. The value of the particle mass flux simulated using the full Lagrangian approach (dashed lines *3* in Fig. 6) agrees better with data of [4, 5] in the first two cross sections, and it is approximately 15 % higher than the mass flux obtained using the Eulerian description (solid lines *2* in Fig. 6). Accordingly, the value of axial velocity of particles calculated by the Lagrangian approach is slightly higher than the corresponding value obtained by the Eulerian method. This conclusion is confirmed by the data shown in Figs. 2–4; according to these data, particle concentration predicted by the Lagrangian method is higher than concentration determined by the Eulerian method.

## Conclusion

Dispersed phase dynamics in a turbulent two-phase swirling flow is studied numerically in the presence of a sudden tube expansion using the Eulerian and Lagrangian methods for describing the two-phase flow.

A significant increase in dispersed phase concentration in the axial zone of the tube in a swirling flow is shown with an increase in the swirl parameter (more than twofold in comparison with a non-swirling separated flow). The reason for this is the action of centrifugal forces and forces of turbulent migration of particles (turbophoresis). As the particle size increases, the particles can be not involved into the separated swirling flow and maintain a positive value of the averaged axial velocity along the entire length of the calculation region. Due to the inertia of particles, the zone of recirculating flows for the dispersed phase is noticeably smaller in comparison with the gas phase recirculation zone.

Good agreement with the measurement data obtained using the Eulerian and full Lagrangian methods [4, 5] was achieved for the averaged characteristics of the two-phase swirling flow and dispersed phase mass flux (the difference between the measured and predicted parameters did not exceed 15 %). In general, both approaches produce similar results. According to the data, it is difficult to draw a conclusion about the advantage of one of the methods for modeling the dispersed phase. The detailed comparative investigation is required, and this is beyond the scope of this paper.

## References


1. **S.S. Kutateladze, E.P. Volchkov, and V.I. Terekhov,** Aerodynamics and Heat and Mass Transfer in Confined Vortex Flows, IT SB AS USSR, Novosibirsk, 1987.
2. **A. Gupta, D. Lilley, and N. Syred,** Swirl Flows, Abacus Press, Tunbridge Wells, 1984.
3. **A.A. Khalatov,** Theory and Practice of Swirling Flows, Naukova Dumka, Kiev, 1989.
4. **M. Sommerfeld and H.-H. Qiu,** Detailed measurements in a swirling particulate two-phase flow by a phase-Doppler anemometer, Int. J. Heat Fluid Flow, 1991, Vol. 12, P. 20–28.
5. **M. Sommerfeld and H.-H. Qiu,** Characterization of particle-laden, confined swirling flow by phase-doppler anemometer and numerical calculation, Int. J. Multiphase Flow, 1993, Vol. 19, P. 1093–1127.
6. **J.P. Jing, Z.Q. Li, L. Wang, Z.C. Chen, L.Z. Chen, and F.C. Zhang,** Influence of the mass flow rate of secondary air on the gas/particle flow characteristics in the near-burner region of a double swirl flow burner, Chem. Engng Sci., 2011, Vol. 66, P. 2864–2871.
7. **L.I. Seleznev and S.G. Tsvigun,** Investigation of the influence of the conditions of swirling on the structure of a two-phase flow in an expanding channel, Fluid Dynamics, 1983, No. 5. P. 729–734.
8. **M. Sommerfeld, A. Ando, and D. Wennerberg,** Swirling, particle-laden flows through a pipe expansion, ASME J. Fluids Engng, 1992, Vol. 114, P. 648–656.
9. **A.A. Vinberg, L.I. Zaichik, and V.A. Pershukov,** Calculation of two-phase swirling flows, Fluid Dynamics, 1994, No.1, P. 55–60.
10. **L.X. Zhou, C.M. Liao, and T. Chen,** Simulation of strongly swirling turbulent gas-particle flows using USM and $k$-$\varepsilon$-$k_P$ two-phase turbulence models, Powder Techn., 2001, Vol. 114, P. 1–11.
11. **M. Sijercic and F. Menter,** Numerical grid refinement in modeling two-phase swirl flow, Thermophysics and Aeromechanics, 2003, Vol. 10, No. 2, P. 163–174.
12. **S.V. Apte, K. Mahesh, P. Moin, and J.C. Oefelein,** Large-eddy simulation of swirling particle-laden flows in a coaxial-jet combustor, Int. J. Multiphase Flow, 2003, Vol. 29, P. 1311–1331.
13. **Y. Liu, L.X. Zhou, and C.X. Xu,** Numerical simulation of instantaneous flow structure of swirling and non-swirling coaxial-jet particle-laden turbulence flows, Physica A, 2010, Vol. 389, P. 5380–5389.
14. **A.V. Shvab and N.S. Evseev,** Studying the separation of particles in a turbulent vortex flow, Theor. Found. Chem. Engng, 2015, Vol. 49, No. 2, P. 191–199.
15. **M.A. Pakhomov and V.I. Terekhov,** Numerical simulation of turbulent swirling gas-dispersed flow behind a sudden tube expansion, Thermophysics and Aeromechanics, 2015, Vol. 22, No. 5, P. 597–608.
16. **D.A. Drew,** Mathematical modeling of two-phase flow, Ann. Rev. Fluid Mech., 1983, Vol. 15, P. 261–291.
17. **R.I. Nigmatulin,** Dynamics of Multiphase Media, CRC Press, 1990.
18. **I.V. Derevich,** Spectral diffusion model of heavy inertial particles in a random velocity field of the continuous medium, Thermophysics and Aeromechanics, 2015, Vol. 22, No. 2, P. 143–162.
19. **D.Ph. Sikovsky,** Singularity of inertial particle concentration in the viscous sublayer of wall-bounded turbulent flows, Flow, Turbulence and Combustion, 2014, Vol. 92, P. 41–64.
20. **S. Jakirlic, K. Hanjalic, and C. Tropea,** Modeling rotating and swirling turbulent flows: a perpetual challenge, AIAA J., 2002, Vol. 40, P. 1984–1996.
21. **S. Fu, P.G. Huang, B.E. Launder, and M.A. Leschziner,** A comparison of algebraic and differential second-moment closures for axisymmetric turbulent shear flows with and without swirl, ASME J. Fluids Engng, 1988, Vol. 110, P. 216–221.
22. **A.M. Jawarneh and G.H. Vatistas,** Reynolds stress model in the prediction of confined turbulent swirling flows, ASME J. Fluids Engng, 2006, Vol. 128, P. 1377–1388.
23. **X.-Q. Chen and J.C.F. Pereira,** Prediction of evaporating spray in anisotropically turbulent gas flow, Numerical Heat Transfer A, 1995, Vol. 27, P. 143–162.
24. **D.B. Taulbee, F. Mashayek, and C. Barre,** Simulation and Reynolds stress modeling of particle-laden turbulent shear flows, Int. J. Heat Fluid Flow, 1999, Vol. 20, P. 368–373.
25. **N. Beishuizen, B. Naud, and D. Roekaerts,** Evaluation of a modified Reynolds stress model for turbulent dispersed two-phase flows including two-way coupling, Flow, Turbulence and Combust, 2007, Vol. 79, P. 321–341.
26. **D.W. Meyer,** Modelling of turbulence modulation in particle- or droplet-laden flows, J. Fluid Mech., 2012, Vol. 706, P. 251–273.
27. **Z.F. Tian, J.Y. Tu, and G.H. Yeoh,** Numerical simulation and validation of dilute gas-particle flow over a backward-facing step, Aerosol Sci. Techn., 2005, Vol. 39, P. 319–332.
28. **P. Frawley, A.P. O'Mahony, and M. Geron,** Comparison of Lagrangian and Eulerian simulations of slurry flows in a sudden expansion, ASME J. Fluids Engng, 2010, Vol. 132, Paper 091301.
29. **M.A. Pakhomov and V.I. Terekhov,** Comparison of the Eulerian and Lagrangian approaches in studying the flow pattern and heat transfer in a separated axisymmetric turbulent gas-droplet flow, J. Appl. Mech. Tech. Phys., 2013, Vol. 54, No. 4, P. 596–607.
30. **A. Fadai-Ghotbi, R. Manceau, and J. Boree,** Revisiting URANS computations of the backward-facing step flow using second moment closures. Influence of the numerics, Flow, Turbulence and Combust, 2008, Vol. 81, P. 395–410.
31. **R. Manceau and K. Hanjalic,** Elliptic blending model: a new near-wall Reynolds-stress turbulence closure, Phys. Fluids, 2002, Vol. 14, P. 744–754.

**32. L.I. Zaichik,** A statistical model of particle transport and heat transfer in turbulent shear flows, Phys. Fluids, 1999, Vol. 11, P. 1521–1534.
**33. I.V. Derevich,** Statistical modelling of mass transfer in turbulent two-phase dispersed flows. 1. Model development, Int. J. Heat Mass Transfer, 2000, Vol. 43, P. 3709–3723.
**34. C.T. Crowe, M.P. Sharma, and D.E. Stock,** The particle source in cell (PSI-Cell) method for gas-droplet flows, ASME J. Fluids Engng, 1977, Vol. 99, P. 325–332.
**35. A.D. Gosman and E. Ioannides,** Aspects of computer simulation of liquid-fuelled combustors, J. Energy, 1983, Vol. 7, P. 482–490.
**36. C.K. Chan, H.Q. Zhang, and K.S. Lau,** An improved stochastic separated flow model for turbulent two-phase flow, Comp. Mech., 2000, Vol. 24, P. 491–502.
**37. P.G. Saffman,** The lift on a small sphere in a slow shear flow, J. Fluid Mech., 1965, Vol. 22, P. 385–400.
**P.G. Saffman,** Corrigendum. "The lift on a small sphere in a slow shear flow, J. Fluid Mech., 1965, Vol. 22, P. 385–400, J. Fluid Mech., 1968. Vol. 31, P. 624.
**38. L.I. Zaichik, V.M. Alipchenkov, and A.R. Avetissian,** A statistical model for predicting the heat transfer of solid particles in turbulent flows, Flow, Turbulence and Combust., 2011, Vol. 86, P. 497–518.
**39. J.-P. Minier, E. Peirano, and S. Chibbaro,** PDF model based on Langevin equation for polydispersed two-phase flows applied to a bluff-body gas-solid flow, Phys. Fluids, 2004, Vol. 16, P. 2419–2431.
**40. E. Amani and M.R.H. Nobari,** Systematic tuning of dispersion models for simulation of evaporating sprays, Int. J. Multiphase Flow, 2013, Vol. 48, P. 11–31.
**41. S. Moissette, B. Oesterle, and P. Boulet,** Temperature fluctuations of discrete particles in a homogeneous turbulent flow: a Lagrangian model, Int. J. Heat Fluid Flow, 2001, Vol. 22, P. 220–226.
**42. J. Pozorski and J.-P. Minier,** On the Lagrangian turbulent dispersion models based on the Langevin equation, Int. J. Multiphase Flow, 1998,Vol. 24, P. 913–945.
**43. T.L. Bocksell and E. Loth,** Stochastic modeling of particle diffusion in a turbulent boundary layer, Int. J. Multiphase Flow, 2006, Vol. 32, P. 1234–1253.
**44. A.N. Osiptsov,** Lagrangian modeling of dust admixture in gas flows, Astrophysics Space Sci., 2000, Vol. 274, P. 377–386.
**45. D.P. Healy and J.B. Young,** Full Lagrangian methods for calculating particle concentration fields in dilute gas-particle flows, Proc. Royal Society A, 2005, Vol. 461, P. 2197–2225.
**46. K. Hanjalic and S. Jakirlic,** Contribution towards the second-moment closure modelling of separating turbulent flows, Computers & Fluids, 1998, Vol. 27, P. 137–156.
**47. P.A. Dellenback, D.E. Metzger, and G.P. Neitzel,** Measurements in turbulent swirling flow through an abrupt axisymmetric expansion, AIAA J., 1989, Vol. 26, P. 669–681.
**48. J.R. Fessler and J.K. Eaton,** Turbulence modification by particles in a backward-facing step flow, J. Fluid Mech., 1999, Vol. 314, P. 97–117.
**49. A.Yu. Varaksin,** Fluid dynamics and thermal physics of two-phase flows: problems and achievements, High Temperature, 2013, Vol. 51, No. 3, P. 377–407.
**50. E.P. Volchkov, L.I. Zaichik, and V.A. Pershukov,** Simulation of Solid Fuel Combustion, Nauka, Moscow, 1994.